Science

AAAS

Pattern Separation in the Dentate Gyrus and CA3 of the Hippocampus
Jill K. Leutgeb *et al.*
Science **315**, 961 (2007);
DOI: 10.1126/science.1135801

This copy is for your personal, non-commercial use only.

Pattern Separation in the Dentate Gyrus and CA3 of the Hippocampus

Jill K. Leutgeb, Stefan Leutgeb, May-Britt Moser, Edvard I. Moser*

Theoretical models have long pointed to the dentate gyrus as a possible source of neuronal pattern separation. In agreement with predictions from these models, we show that minimal changes in the shape of the environment in which rats are exploring can substantially alter correlated activity patterns among place-modulated granule cells in the dentate gyrus. When the environments are made more different, new cell populations are recruited in CA3 but not in the dentate gyrus. These results imply a dual mechanism for pattern separation in which signals from the entorhinal cortex can be decorrelated both by changes in coincidence patterns in the dentate gyrus and by recruitment of nonoverlapping cell assemblies in CA3.

The formation of discrete representations in memory is thought to depend on a pattern separation process whereby cortical inputs are decorrelated as they enter the early stages of the hippocampus (1–4). The neuronal mechanisms of hippocampal pattern separation have remained elusive, however. In principle, new representations could be distinguished merely as a result of attractor dynamics in the associative CA3 network (1–3, 5–7), but because CA3 cells are strongly controlled by other CA3 cells, via recurrent collaterals, the CA3 area on its own may have limited ability to generate new representations in response to weak

Centre for the Biology of Memory, Norwegian University of Science and Technology, 7489 Trondheim, Norway.

*To whom correspondence should be addressed. E-mail: edvard.moser@ntnu.no

changes in cortical input. Instead, small changes might result in the retrieval of similar patterns that have already been stored in the network (pattern completion) (1–3, 5–9). The formation of novel discrete representations would benefit strongly from the existence of an additional neuronal layer, upstream of CA3, where small differences between incoming signals could be augmented before the input is presented to the associative network. The dentate gyrus has been proposed to serve such a function (1–4). On the basis of analogies with the cerebellum (10–12), it has been suggested that, in the dentate gyrus, input from the entorhinal cortex is dispersed onto a more extensive layer of sparsely firing granule cells, enabling each granule cell to carry only a small and distinct fraction of the total input (1). By way of the sparse level of firing in the granule cell population (13, 14) and the

sparse connections between the granule cells and the pyramidal cells in CA3 (15), the segregation of incoming inputs from the cortex might be retained as the inputs enter the CA3 network. The proposed role of the dentate gyrus in pattern separation can be tested experimentally by measuring the ability of dentate neurons to disambiguate small differences in cortical input patterns. In both the dentate gyrus and the CA areas, the principal cells have spatial receptive fields, i.e., they discharge only when the animal is in particular places (13, 16, 17). In the CA areas, pattern separation is expressed in place cells as a substantial reorganization of the collective firing pattern ("remapping") that is induced when sensory or motivational inputs to the network exceed a certain difference threshold (18–25). To establish whether a similar ability to distinguish overlapping input patterns is expressed in the dentate gyrus, we compared the transformation of representations in the dentate gyrus and CA3 under conditions where sensory input patterns were made progressively more different.

Six rats were trained to run in square or circular enclosures. During running, spikes were sampled from putative pyramidal cells in CA3 ($n = 216$) and granule cells in the dentate gyrus ($n = 67$) (Fig. 1, A and B, and fig. S1 and table S1) (25). In five of the animals, data were recorded simultaneously from the two areas. The number of active cells was lower in the dentate gyrus than in CA3 (25), which confirmed previous indications of sparse firing in the granule cell population (13, 14), but among those neurons that were active, the peak firing rates were similar in the two hippocampal regions [$t = 0.95$, df = 94, not significant (n.s.)

Fig. 1. Place-specific firing in (**A**) the pyramidal layer of CA3, and (**B**) the granule layer of the dentate gyrus. (A) and (B) were recorded simultaneously (rat 11215) (See fig. S1 for additional electrode positions from this animal). (Left) Recording locations (arrow) identified by following the electrode tracts through serial cresyl violet–stained sections. DG, dentate gyrus. (Middle) Cluster diagrams showing separation of extracellular action potentials (spikes) when the animal foraged in a square box for 10 min or when the animal slept. Scatterplots show energies (sum of squares) of waveforms on two recording channels. Each dot represents one sampled spike. Distinct spike clusters (each corresponding to one putative cell) are assigned a unique color that is consistent across pairs of cluster diagrams. Insets show the spikes from the red cluster superimposed on the rat's trajectory (gray) during food-motivated running in a square enclosure. (Right) Waveforms of spikes from the red clusters (means ± standard deviation). Bottom of each panel, representative EEG trace from the indicated recording site during foraging in the box.
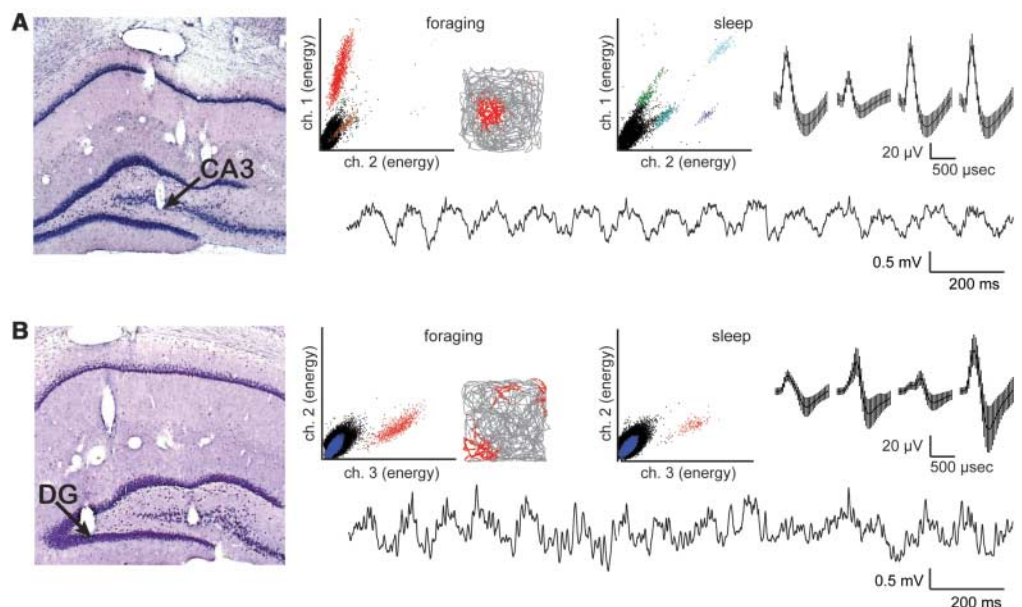
(table S1)]. The majority of active cells exhibited strongly localized firing in both areas. Of the 71 active CA3 cells, 62 (87.3%) had localized firing; 58 cells had a single field and only 4 had more than one firing field (Fig. 1A). Of the 44 active dentate cells, 41 had firing fields. The majority of these cells fired at multiple places [16 had single fields, 13 double fields, 8 triple fields, and 4 quadruple fields (Fig. 1B and fig. S2)] (13, 14). The distribution of the multiple firing fields was generally irregular (Fig. 1B).

Pattern separation by changes in spatial and temporal coincidence. We compared the activity of simultaneously recorded principal neurons from dentate gyrus and CA3 during incremental transformation of the recording environment. Five rats were first trained in square and circular versions of a recording enclosure with flexible walls, with the two versions presented in random order (26) (fig. S3). The box was then transformed, through a series of five intermediate shapes, from the square shape to the circular shape ($n = 57$ dentate and 170 CA3 cells) or vice versa ($n = 66$ dentate and 186 CA3 cells) (Fig. 2A; fig. S4 and S5). The transformation was accompanied by a progressive change in the firing rate distribution of cells in both CA3 and dentate gyrus. In the dentate gyrus, the multiple firing fields of each cell changed noncoherently; some were most active in the initial shape, others in the middle or final shapes (Fig. 2, B and C). These differential changes resulted in a strong decorrelation of the rate distribution of individual cells between even the closest shapes of the morph box. The rate distribution changed independently of the order of the box shapes (fig. S6), unlike the firing rates in CA3, which exhibited hysteresis (Fig. 2B and fig. S6) (26).

To examine how the decorrelation of discharge patterns in the dentate gyrus might influence CA3, we estimated the cumulative change in population output from the dentate gyrus as increasing degrees of dissimilarity were introduced between pairs of test boxes.

Fig. 2. Changes in rate distribution in CA3 and dentate gyrus during progressive transformation of the recording environment. (**A**) Cells were recorded consecutively in seven shapes of an enclosure with flexible walls, starting with a square (1) and ending with a circle (7), or vice versa. The initial shape was finally repeated (1'). (**B**) Firing fields for a representative CA3 cell (top, purple box) and a simultaneously recorded cell in the dentate gyrus (bottom, green box). (Left) Trajectories with spike locations; (right) corresponding color-coded rate maps. The color scale is from blue (silent) to red (peak rate), with pixels not visited shown in white. The rate maps were scaled to the maximum firing rate within the entire testing sequence. Peak rates are indicated to the right. The complete set of active cells is shown in fig. S4. (**C**) Differential rate changes in individual firing fields of the cell in (B) and two additional representative cells from the dentate gyrus (from different animals). Individual fields of each cell are outlined in different, but consistent, colors throughout the morph sequence. (Right) Line diagrams for the mean firing rate (red curve) in each individual firing field (box outlines have the same color as the corresponding firing fields). The rates were fitted to sigmoid, linear, or quadratic functions. Curve fits are only shown when significant (in black). The best fit was linear for 30 fields, sigmoidal for 21 fields, and quadratic for 8 fields ($n = 122$).
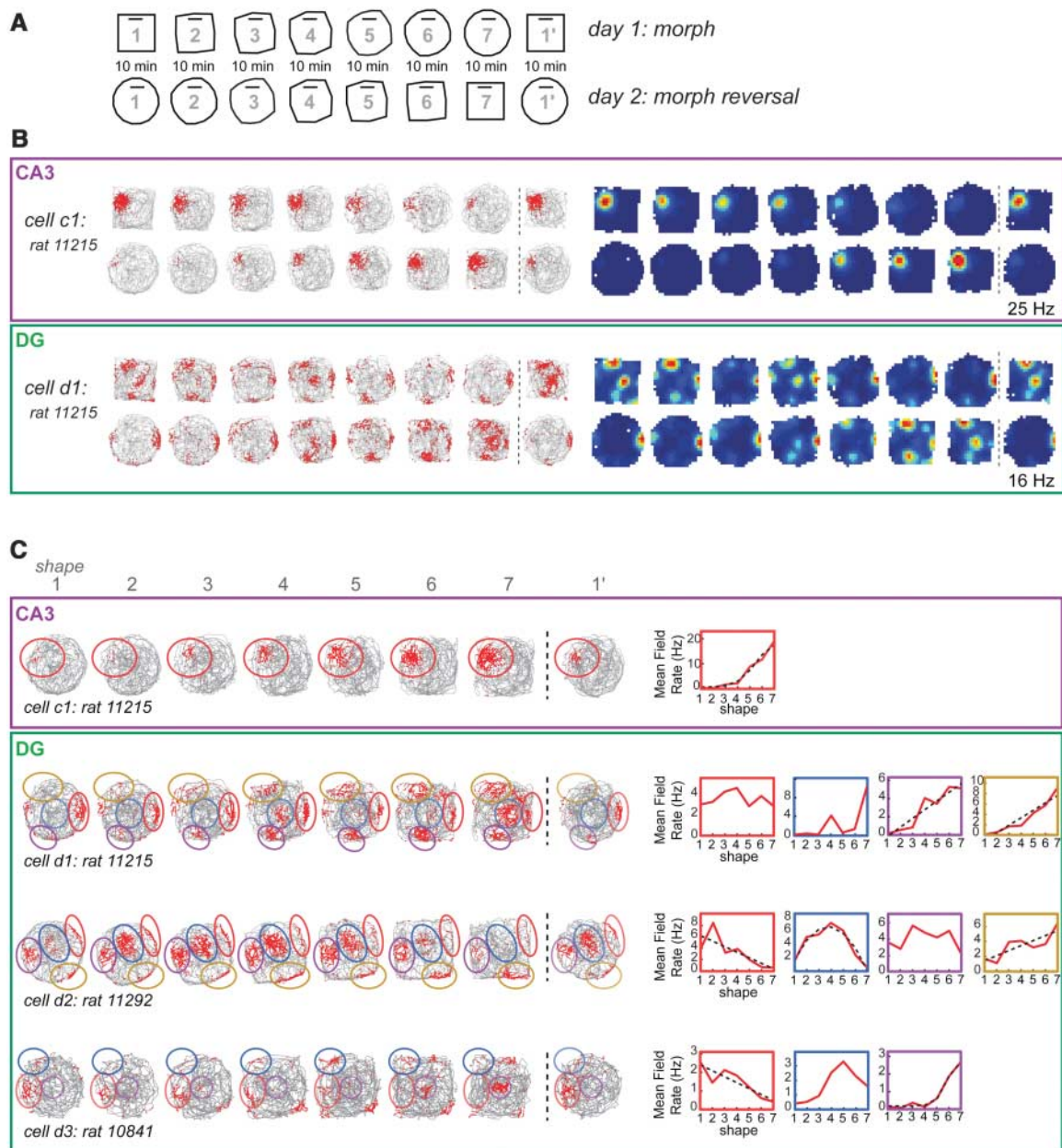
Composite population vectors were constructed for each box by stacking the rate maps of all cells into a three-dimensional matrix with the two spatial dimensions discretized along the x and y axes and cell identity represented on the z axis (Fig. 3A). For each pair of environments, the firing rates of the active cells were correlated for each spatial bin shared by the two box shapes. Population activity in the dentate gyrus was highly sensitive to small changes in the shape of the environment (Fig. 3A). The smallest difference gave a highly significant decrease in the correlation of the population vectors for the dentate gyrus (0.75 ± 0.01 for shape 1 versus 2 and 0.87 ± 0.004 for shape 1 versus 1'; mean correlation $\pm$ SEM, $t = 15.1$, $P < 0.001$). A similar decrease was not observed in CA3, where the population vector correlations for neighboring shapes and identical shapes were about the same (0.92 ± 0.004 and 0.92 ± 0.003, respectively, $t = 1.96$, n.s.). As the shapes
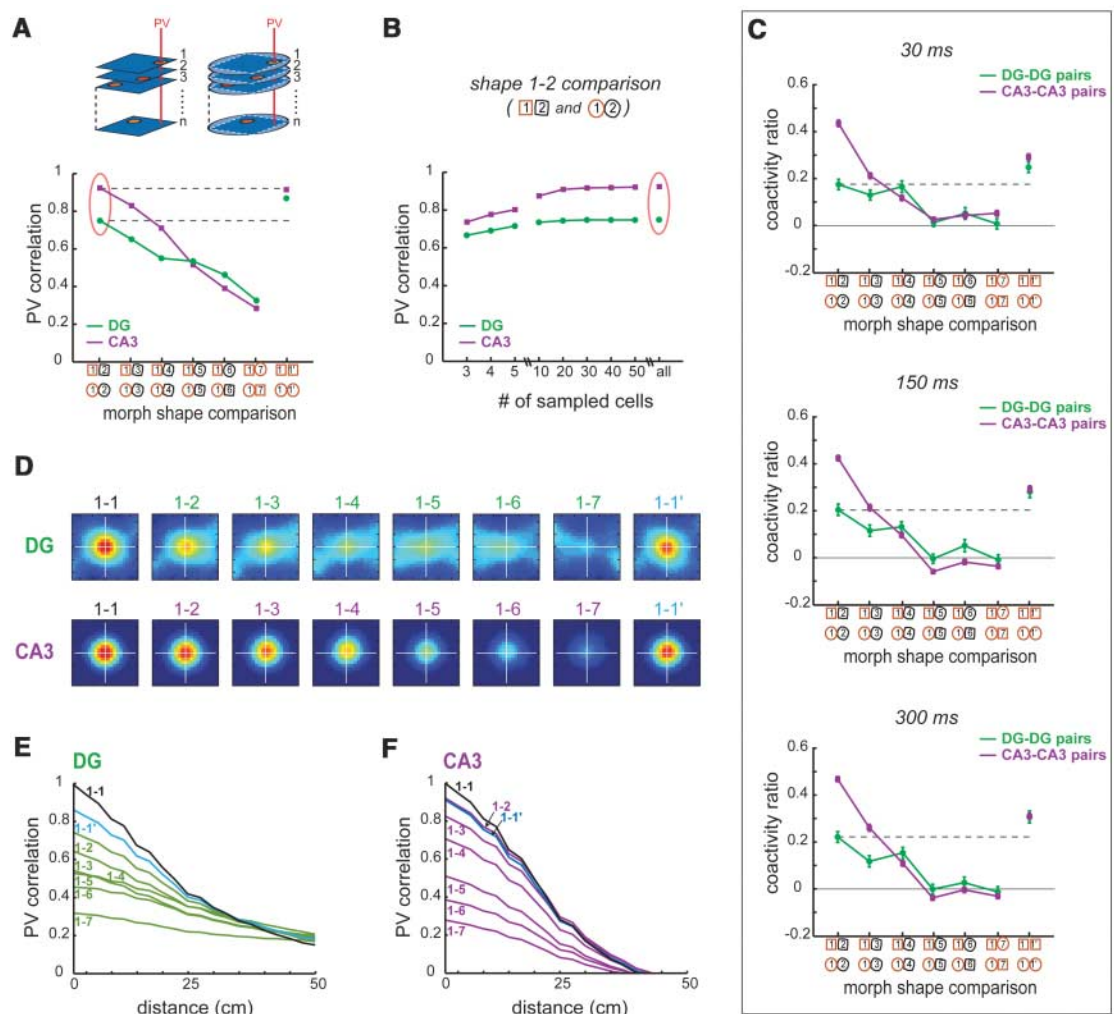
became more different, the correlations decreased in both hippocampal subfields, but the decrease was initially more pronounced in the dentate gyrus (Fig. 3A). The advance of the dentate gyrus disappeared toward the end of the morph sequence. Because the impact of decorrelation processes in the dentate gyrus is likely to be constrained by the limited convergence of granule cells on CA3 neurons (15, 27), we asked whether a similar distinction between adjacent shapes would be possible with sparser inputs. The change in spatial population vectors in the dentate gyrus was thus calculated after subsampling from the recorded cell population. Small changes in box shape (1 versus 2) led to a similar drop in correlation even when the cell sample was reduced to less than 10 (Fig. 3B and fig. S7).

The differentiation of the spatial rate maps could be improved by decorrelation in the temporal domain (28). For each pair of simultaneously recorded cells, we thus determined the

rate of coincident firing within time windows of 30 ms, 150 ms, and 300 ms (25). The coincidence rates, averaged across cell pairs, were compared for successive shapes of the morph sequence by dividing the rates by each other, giving a coactivity ratio. The coactivity ratio decreased across morph trials and, in the dentate gyrus, dropped significantly even between adjacent shapes (Fig. 3C and fig. S8). The decrease between shapes 1 and 2 was significant for all three time windows ($t > 2.14$, $P < 0.05$). For larger shape differences, the dissimilarity reached the level of a shuffled distribution (0 in Fig. 3C). Cell pairs in CA3 were more correlated than cell pairs with one cell from the dentate gyrus and one from CA3 (fig. S8).

We next asked whether the change in the representation of the environment in the dentate gyrus bears any qualitative similarity to remapping processes in the CA fields. In place cells in CA3, and to some extent in CA1, remapping

Fig. 3. Quantitative assessment of spatial and temporal coincidence reduction in the dentate gyrus. (**A**) (Top) Procedure for calculating population vector correlations. The rates of all CA3 or dentate cells were stacked into 256 population vectors (PVs), one for each of the 5 cm by 5 cm bins that were shared between the morph square and the morph circle. The correlation between the population vectors was computed for each pair of pixels. (Bottom) Mean population vector correlations for pairs of increasingly divergent morph shapes. Unlike the population output from CA3, population vectors in the dentate gyrus showed dissimilarities already at the smallest change of the box configuration (shape 1 versus 2). (Gray stippled lines highlight the difference between this comparison and repeated recordings in shape 1.) (**B**) Population vector correlations after random subsampling from the recorded cell sample. Subsets of cells were chosen from either dentate gyrus or CA3, and correlation coefficients were calculated as in (A). Corresponding data points in (A) and (B) are circled in red. (**C**) Change in temporal correlation of cell pairs as a function of difference between morph shapes. The degree of change across morph shapes was expressed as the ratio, for each cell pair, of coactive spikes in one environment divided by coactive spikes in the other, within three time windows as noted. The ratio is averaged and linearly transformed such that randomly shuffled cell pairs have a ratio of 0. Symbols as in (A). (**D**) Color-coded spatial cross-correlation matrices for composite rate maps, one for each pair of morph shapes. The scale is from red (+1) to blue ($\leq$0); yellow corresponds to 0.5 to 0.7. (**E** and **F**) Line diagrams showing cross-correlations as a function of distance from the center of the cross-correlogram for pairs of trials with increasing dissimilarity in box shape [one line for each pair; (E), dentate gyrus; (F), CA3].

occurs as a complete change in both firing fields and firing rates ("global remapping") or as a selective change in firing rates within a fixed set of firing locations ("rate remapping") (24, 29). In the present study, the CA3 neurons exhibited consistent rate remapping throughout the morph sequence (26), whereas cells from the dentate gyrus fired at different locations in the most different shapes of the box (Fig. 2B). Yet, the redistribution of the firing locations was non-random. In all individual fields of a dentate neuron, firing increased and decreased gradually across multiple trials, sometimes throughout the entire morph sequence (Fig. 2C). To estimate the extent to which the place code was retained, as in the CA3 cells, we cross-correlated the composite rate maps of the dentate cells for each pair of shapes in the morph sequence by shifting the stack from one of the shapes in 5-cm steps along the x and y axes. This resulted in a map of the average similarity of the population vectors, at various shifts of one stack relative to the other. A central peak was observed for all pairs of shapes, but the peak decreased progressively as the shapes became more different (Fig. 3, D to F), which suggested that the rate distribution was altered smoothly, as during rate remapping in CA3 (26). Even the smallest shape change caused a decrease in the central peak in the dentate gyrus (see also Fig. 3A).

The expression of a coactivity-based pattern separation process in the dentate gyrus raises the question of whether the underlying computa-

tions take place locally in the dentate gyrus or are mediated from afferent regions. If the dentate gyrus contributes actively to pattern separation, its sensitivity to small changes in input patterns should be substantially larger than in the entorhinal cortex, which mediates the majority of cortical inputs to this area. We tested this prediction by recording from three cells in the perforant-path termination area of the hippocampus while the shape of the recording box was increased in small steps (Fig. 4 and fig. S9). These cells had grid-like firing fields similar to those of principal cells in the medial entorhinal cortex (30, 31). The spikes may have originated from intact or punctured axons of grid cells or, perhaps, but less likely, from local interneurons activated by grid cells with identical firing locations. The three cells were recorded simultaneously with cells in the granule cell layer on other tetrodes. None of the grid cells exhibited detectable changes in the rate or the location of firing that could be attributed to the incremental transformation of the recording environment (Fig. 4, B and C, and fig. S9). Whereas the magnitude of the cross-correlation between pairs of environments decreased progressively in the simultaneously recorded dentate neurons, the correlation did not change systematically for the grid cells (Fig. 4C). These recordings confirm observations from studies with larger numbers of entorhinal grid cells, which show that the distribution of activity between firing fields in entorhinal neurons does not change detectably in

response to environmental reconfiguration under conditions where hippocampal CA3 assemblies undergo rate remapping (32).

Pattern separation by recruitment of new cell assemblies. Although changes in the shape of the morph box strongly influenced the co-activity of already active neurons in the dentate gyrus, there was no replacement of the active subset of the population. In CA3, such replacement can be induced by further increasing the differences between the environments, either by moving the animal to a different recording room (24, 33) or by making the enclosures more dissimilar (18, 19, 23, 32). We asked whether such changes, sufficient to induce global remapping in the CA3 (24), would cause new and independent cell ensembles to be recruited also in the dentate gyrus. Rats were tested in boxes of different size, color, and shape in three different rooms (Fig. 5, and figs. S10 and S11). As expected, in CA3, statistically independent sub-populations were recruited in a pair of similarly shaped rooms (33) (Fig. 5). With a rate threshold of 0.1 Hz, only 20 (18.3%) of the 109 CA3 cells that were active in one room were also active in the second room. Of the 23 active CA3 cells recorded simultaneously with dentate cells, only 3 (13.0%) were active in both rooms (table S1). In striking contrast, 17 out of 20 active neurons in the dentate gyrus (85.0%) were active in both room 1 and room 2; only three (each from a different animal) fired exclusively in one of the environments (Fig. 5). The regional difference
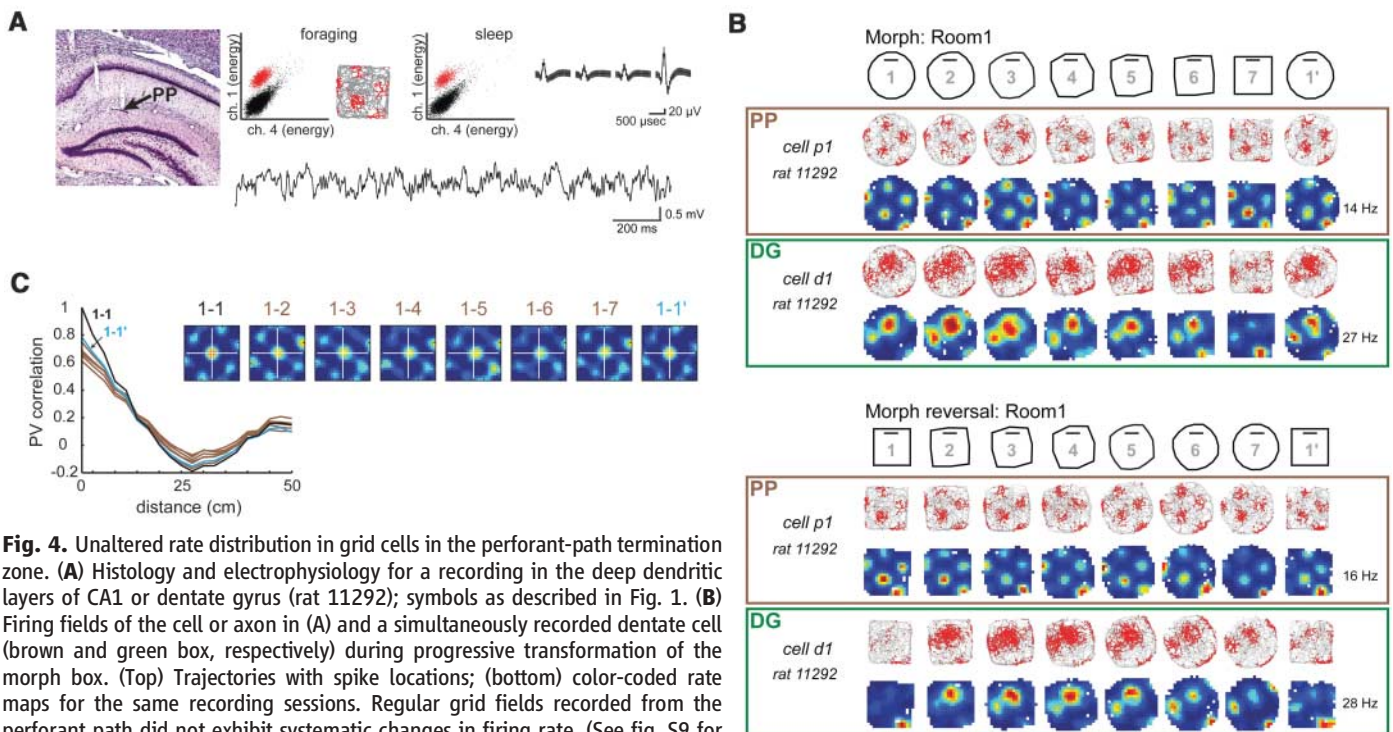
Fig. 4. Unaltered rate distribution in grid cells in the perforant-path termination zone. (**A**) Histology and electrophysiology for a recording in the deep dendritic layers of CA1 or dentate gyrus (rat 11292); symbols as described in Fig. 1. (**B**) Firing fields of the cell or axon in (A) and a simultaneously recorded dentate cell (brown and green box, respectively) during progressive transformation of the morph box. (Top) Trajectories with spike locations; (bottom) color-coded rate maps for the same recording sessions. Regular grid fields recorded from the perforant path did not exhibit systematic changes in firing rate. (See fig. S9 for additional examples.) (**C**) Cross-correlation between rate maps for grid cells in the perforant-path termination zone, calculated as in Fig. 3, D to F, and shown for incremental changes in box shape. The line diagram shows a central peak, as expected if the fields remain stable, and a second peak at 45 to 50 cm from the center, which is a consequence of the similar grid spacing (40 to 60 cm) of the recorded grid cells. PP, perforant path.

was highly significant ($Z = 22.0$, $P < 0.001$, simultaneously recorded cells only). The difference was maintained with a higher rate threshold [0.25 Hz; $Z = 20.8$; $P < 0.001$ (table S1)] and with a rate overlap measure where, for each cell, the mean firing rate in the less-active setting was divided by the mean rate in the more-active setting (33) [$t = 4.77$, $P < 0.001$ (fig. S10)]. Moreover, in two animals that were tested in a third room where the enclosure was substantially larger, 11 out of 12 dentate cells that were active in rooms 1 and 2 were active also in room 3 (fig. S11). Although the active subset was generally the same in all three rooms, there was no similarity in the relative locations of their firing fields. Irrespective of the relative orientation of the stacks, cross-correlation maps for simultaneously recorded dentate neurons in rooms 1 and 2 were flat, and the coactivity of cell pairs was

not higher than that of a shuffled rate distribution (Fig. 5D and fig. S12).

Discussion. This study provides experimental support for a role of the initial stages of the hippocampus in pattern separation and suggests that a dual set of network mechanisms is involved. These mechanisms, implemented in the dentate gyrus and CA3, are both able, in different ways, to completely orthogonalize the collective firing pattern of cell assemblies in CA3. Together they provide a potential neuronal substrate for disambiguation of overlapping memories in the hippocampus.

Which mechanism is recruited depends on the nature of changes in inputs to the hippocampus. When the environment is only slightly modified, at a fixed spatial location, pattern separation is expressed in dentate gyrus and CA3 as a change in the pattern of correlated

activity within the active cell assembly. The divergent direction of the rate changes in the different firing fields of dentate cells accentuates the decorrelation of the ensemble activity, which allows each environment to be represented by a unique rate pattern in a small number of granule cells. Sparse connections between granule cells in the dentate gyrus and pyramidal cells in CA3 (15) may allow the disambiguation of firing patterns to be translated to the CA fields, although the smallest differences may be opposed by pattern completion processes in the CA3 network (2, 3, 5–9). Whether decorrelation in the dentate gyrus is necessary for rate redistribution in the CA fields remains to be determined. When the changes in input to the hippocampus are more substantial, pattern separation is accomplished also by recruitment of a statistically independent cell population in CA3 (24, 33, 34).

Fig. 5. Recruitment of statistically independent cell ensembles in CA3, but not in dentate gyrus, after large changes in the recording environment. (**A** and **B**) Firing fields of all cells recorded simultaneously from CA3 (A) and the dentate gyrus (B) in an animal exploring boxes of varied size and color in two different rooms (rat 11215). (A) Recording sequence schematic and spatial firing correlates for active cells recorded from tetrodes in CA3. The rat's trajectory (gray) with superimposed spike locations (red dots) is shown for each cell. Silent cells are not shown ($n = 8$). (B) Trajectories with spike locations for dentate cells recorded simultaneously with the CA3 cells in (A). (See fig. S10 for color-coded rate maps.) (**C**) Relation between firing rates on repeated tests in the same room (blue symbols) or in different rooms (red symbols) for the entire sample of cells recorded in CA3 (top) and dentate gyrus (bottom) ($n = 11$ animals, three with simultaneous recordings). Circles of lighter color indicate cells from trials with simultaneous recording in dentate gyrus and CA3; darkened circles indicate cells that were recorded separately in one brain region. (**D**) Cross-correlation between rate maps for cells with firing fields in both rooms, calculated as in Fig. 3D, but with prior rotation of the maps relative to each other and with analyses performed separately for individual animals. The line diagrams show cross-correlations for individual experiments as a function of distance from the center of the cross-correlogram (one line for each animal with more than three simultaneously recorded cells in either subfield). Cross-correlation maps (at the bottom) are only shown for rat 11215 [corresponding to (A) and (B)]. (See fig. S12 for the remaining maps.)
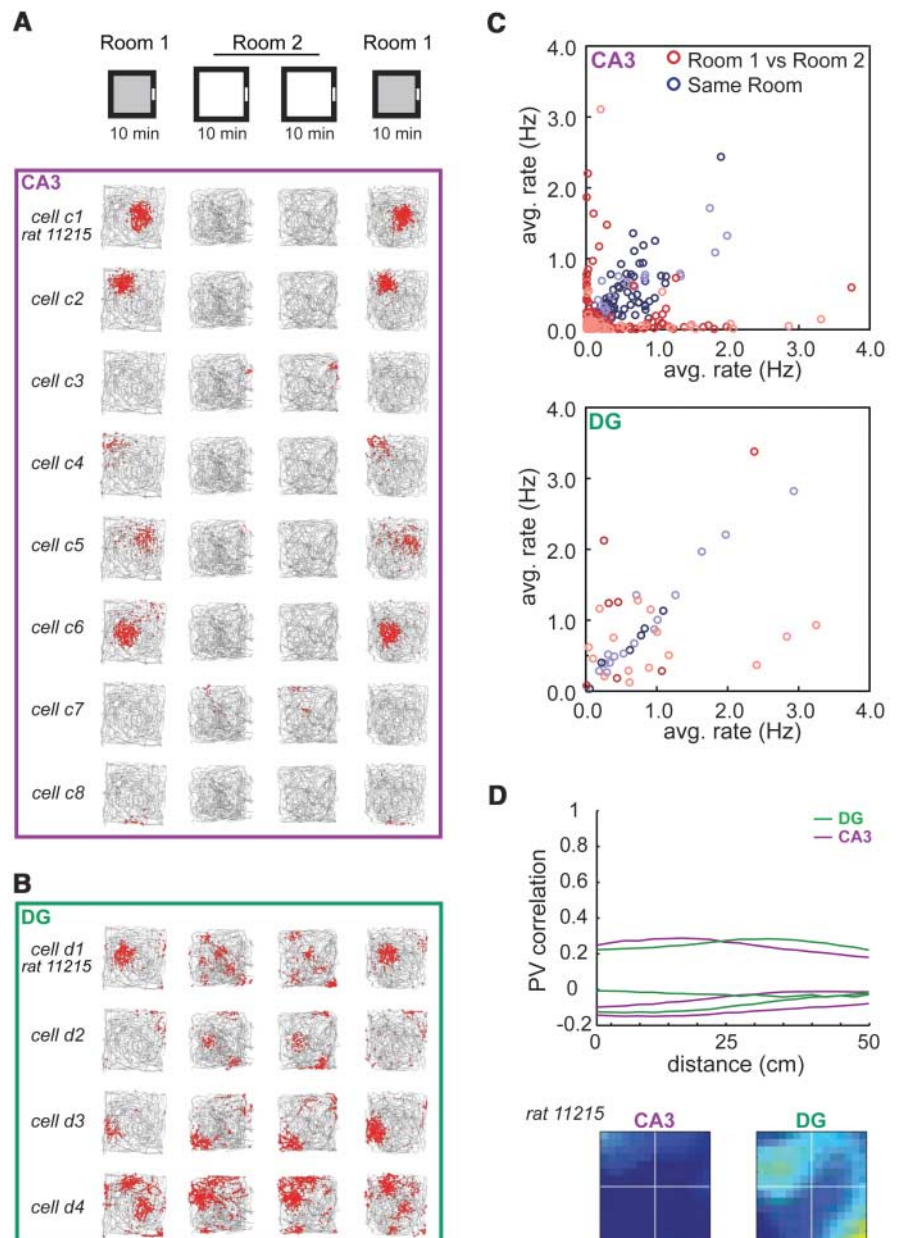
A similar replacement of the active subset is not apparent in the dentate gyrus, which suggests that the change in the CA3 code is triggered by direct projections from entorhinal grid cells to the CA3 (32).

Pattern separation in the dentate gyrus is thus different from separation processes in the cerebellum (10, 11), where signals from the brain stem spread out on a layer of granule cells whose cell numbers exceed those of the input layer by a factor of several million. The number of granule cells in the dentate gyrus and pyramidal cells in the CA3 only marginally outnumbers the projection neurons from layer II of the entorhinal cortex [in the rat, 1,000,000, 300,000 and 200,000, respectively (15, 35, 36)], which suggests that the same hippocampal cells must participate in many representations even when the population activity is sparse (13, 14). In such networks, orthogonalization of coincidence patterns may be more effective.

The decorrelated firing of the dentate cells contrasts with the invariant discharge structure of grid cells upstream in the medial entorhinal cortex (30–32) (Fig. 4). The reduction in spatiotemporal coincidence could be derived from the lateral entorhinal cortex, but not by a straightforward relay mechanism, because cells in this area do not exhibit reliable place modulation (37). It is thus likely that many of the underlying computations take place within the dentate gyrus itself. The use of a dedicated neuronal population for orthogonalization of small differences in input to the CA fields enables the hippocampal network to encode the full variety of experience in a more diversified manner than what could be accomplished with attractor networks alone.

References and Notes

1. B. L. McNaughton, L. Nadel, in *Neuroscience and Connectionist Theory*, M. A. Gluck and D. E. Rumelhart, Eds. (Lawrence Erlbaum, Hillsdale, NJ, 1989), pp. 1–63.
2. A. Treves, E. T. Rolls, *Hippocampus* **2**, 189 (1992).
3. R. C. O'Reilly, J. L. McClelland, *Hippocampus* **4**, 661 (1994).
4. P. E. Gilbert, R. P. Kesner, I. Lee, *Hippocampus* **11**, 626 (2001).
5. D. Marr, *Philos. Trans. R. Soc. Lond. B Biol. Sci.* **262**, 23 (1971).
6. M. E. Hasselmo, E. Schnell, E. Barkai, *J. Neurosci.* **15**, 5249 (1995).
7. M. Tsodyks, *Hippocampus* **9**, 481 (1999).
8. K. Nakazawa et al., *Science* **297**, 211 (2002).
9. I. Lee, D. Yoganarasimha, G. Rao, J. J. Knierim, *Nature* **430**, 456 (2004).
10. D. Marr, *J. Physiol.* **202**, 437 (1969).
11. J. Albus, *Math. Biosci.* **10**, 25 (1971).
12. P. Chadderton, T. W. Margrie, M. Hausser, *Nature* **428**, 856 (2004).
13. M. W. Jung, B. L. McNaughton, *Hippocampus* **3**, 165 (1993).
14. M. K. Chawla et al., *Hippocampus* **15**, 579 (2005).
15. D. G. Amaral, N. Ishizuka, B. Claiborne, *Prog. Brain Res.* **83**, 1 (1990).
16. J. O'Keefe, J. Dostrovsky, *Brain Res.* **34**, 171 (1971).
17. R. U. Muller, J. L. Kubie, J. B. Ranck Jr., *J. Neurosci.* **7**, 1935 (1987).
18. R. U. Muller, J. L. Kubie, *J. Neurosci.* **7**, 1951 (1987).
19. G. J. Quirk, R. U. Muller, J. L. Kubie, *J. Neurosci.* **10**, 2008 (1990).
20. E. Bostock, R. U. Muller, J. L. Kubie, *Hippocampus* **1**, 193 (1991).
21. E. J. Markus et al., *J. Neurosci.* **15**, 7079 (1995).
22. C. Lever, T. Wills, F. Cacucci, N. Burgess, J. O'Keefe, *Nature* **416**, 90 (2002).
23. T. J. Wills, C. Lever, F. Cacucci, N. Burgess, J. O'Keefe, *Science* **308**, 873 (2005).
24. S. Leutgeb et al., *Science* **309**, 619 (2005).
25. Materials and Methods and other supporting material are available on *Science* Online.
26. J. K. Leutgeb et al., *Neuron* **48**, 345 (2005).
27. D. A. Henze, L. Wittner, G. Buzsáki, *Nat. Neurosci.* **5**, 790 (2002).
28. K. D. Harris, J. Csicsvari, H. Hirase, G. Dragoi, G. Buzsáki, *Nature* **424**, 552 (2003).
29. R. M. Hayman, S. Chakraborty, M. I. Anderson, K. J. Jeffery, *Eur. J. Neurosci.* **18**, 2825 (2003).
30. M. Fyhn, S. Molden, M. P. Witter, E. I. Moser, M.-B. Moser, *Science* **305**, 1258 (2004).
31. T. Hafting, M. Fyhn, S. Molden, M.-B. Moser, E. I. Moser, *Nature* **436**, 801 (2005).
32. M. H. Fyhn, T. F. Hafting, A. Treves, E. I. Moser, M.-B. Moser, *Nature,* in press.
33. S. Leutgeb, J. K. Leutgeb, A. Treves, M.-B. Moser, E. I. Moser, *Science* **305**, 1295 (2004).
34. A. Vazdarjanova, J. F. Guzowski, *J. Neurosci.* **24**, 6489 (2004).
35. P. R. Rapp, P. S. Deroche, Y. Mao, R. D. Burwell, *Cereb. Cortex* **12**, 1171 (2002).
36. B. D. Boss, G. M. Peterson, W. M. Cowan, *Brain Res.* **338**, 144 (1985).
37. E. L. Hargreaves, G. Rao, I. Lee, J. J. Knierim, *Science* **308**, 1792 (2005).
38. We thank A. Treves, C. A. Barnes, and M. R. Mehta for discussion and A. M. Amundsgard, K. Haugen, K. Jenssen, E. Sjulstad, R. Skjerpeng, and H. Waade for technical assistance. This work was supported by a Centre of Excellence grant from the Norwegian Research Council.

REPORTS

Experimental Realization of Wheeler's Delayed-Choice Gedanken Experiment

Vincent Jacques,[1] E Wu,[1,2] Frédéric Grosshans,[1] François Treussart,[1] Philippe Grangier,[3] Alain Aspect,[3] Jean-François Roch[1]*

Wave-particle duality is strikingly illustrated by Wheeler's delayed-choice gedanken experiment, where the configuration of a two-path interferometer is chosen after a single-photon pulse has entered it: Either the interferometer is closed (that is, the two paths are recombined) and the interference is observed, or the interferometer remains open and the path followed by the photon is measured. We report an almost ideal realization of that gedanken experiment with single photons allowing unambiguous which-way measurements. The choice between open and closed configurations, made by a quantum random number generator, is relativistically separated from the entry of the photon into the interferometer.

Young's double-slit experiment, realized with particles sent one at a time through an interferometer, is at the heart of quantum mechanics (1). The striking feature is that the phenomenon of interference, interpreted as a wave following two paths simultaneously, is incompatible with our common-sense representation of a particle following one route or the other but not both. Several single-photon interference experiments (2–6) have confirmed the wave-particle duality of the light field. To understand their meaning, consider the single-photon interference experiment sketched in Fig. 1. In the closed interferometer configuration, a single-photon pulse is split by a first beamsplitter BS_{input} of a Mach-Zehnder interferometer and travels through it until a second beamsplitter BS_{output} recombines the two interfering arms. When the phase shift Φ between the two arms is varied, interference appears as a modulation of the detection probabilities at output ports 1 and 2, respectively, as $\cos^2 \Phi$ and $\sin^2 \Phi$. This result is the one expected for a wave, and as Wheeler pointed out, "[this] is evidence … that each ar-

[1]Laboratoire de Photonique Quantique et Moléculaire, Ecole Normale Supérieure de Cachan, UMR CNRS 8537, 94235 Cachan, France. [2]Key Laboratory of Optical and Magnetic Resonance Spectroscopy, East China Normal University, 200062 Shanghai, China. [3]Laboratoire Charles Fabry de l'Institut d'Optique, Campus Polytechnique, UMR CNRS 8501, 91127 Palaiseau, France.

*To whom correspondence should be addressed. E-mail: roch@physique.ens-cachan.fr